Localization of a Scatterer in 3D with a Single Measurement and Single Element Transducer

Luzhen Nie[1], Joshua Tjun Minh Moo[2], Matthieu Toulemonde[3], Meng-Xing Tang[3], Steven Freear[1], and Sevan Harput[4]

[1] School of Electronic and Electrical Engineering, University of Leeds, Leeds, U.K.
[2] School of Biomedical Engineering & Imaging Sciences, King's College London, London, U.K.
[3] Department of Bioengineering, Imperial College London, London, U.K.
[4] Division of Electrical and Electronic Engineering, London South Bank University, London, U.K.
E-mail: harputs@lsbu.ac.uk

***Abstract*—Conventionally an A-mode scan, a single measurement with a single element transducer, is only used to detect the depth of a reflector or scatterer. In this case, a single measurement reveals only one-dimensional information; the axial distance. However, if the number of scatterers in the ultrasonic field is sparse, it is possible to detect the location of the scatter in multiple spatial dimensions. In this study, we developed a method to find the location of a scatterer in 3-D with a single-element transducer and single measurement. The feasibility of the proposed method was verified in 2-D with experimental measurements.**

I. Introduction

Medical ultrasound imaging constitutes an important aid in decision making at the frontline of daily clinical practice, with advantages of being non-radioactive, bedside accessible, affordable, and friendly for long-term surveillance with repetitive scans. The past decades have seen the advances of medical ultrasound imaging technology and devices, from the early development of single-element transducer systems, to the manufacture of 1-D and 2-D array transducer platforms which underpin visualization of the 2-D cross section and 3-D volume, respectively [1]. Constrained by costs and system complexity (data capture, transfer and storage), true volumetric 3-D ultrasound imaging (using more than 1000 sensors) has not gained popularity. To reduce the cost and complexity of the ultrasound systems and the probes, several methods have been proposed. These methods aimed to reduce the number of active elements or channels by using element multiplexing [2], [3], row-column addressed matrix arrays [4], [5] and 2-D sparse arrays [6]–[10]. For a 3-D view of the volume, a 1-D transducer array can be also mechanically translated or rotated, with each 2-D slice gained at each moment/position stacked together [11]–[13]. In recent years, developing simpler, more compact and cheaper devices for 3-D ultrasound imaging has been of great research interest, with promise in broadening the adoption of 3-D ultrasound evaluation [14]–[17]. Of particular prominence is the compressive imaging strategy [14], where a single-element sensor acts as both the transmitter and receiver. A single-element transducer was thought to lack the capability of distinguishing echoes from different incident angles when there were no spatiotemporal variations in the transmitted filed. A rotating coding mask placed in front of the sensor was thus used to remove this ambiguity, by introducing artificial field diversity across the sensor surface in both transmission and reception. This ensured unique echo features for each spatial location in 3D, allowing for decoding 1-D compressive measurements to 3-D visualization using computing power [14].

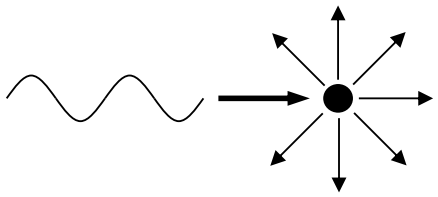

Fig. 1. Illustration of scattering. The sinusoidal pattern represents the propagating ultrasound wave. The thin arrows represent echoes scattered from the sub-wavelength object (black circular region) and the thick arrow indicates the direction of ultrasound propagation.

If the number of scatterers in the ultrasonic field is sparse, it is possible to detect the location of the scatterer in multiple spatial dimensions by using a single-element transducer. In this work, we presented that the location of a scatterer can be detected both in axial direction and a direction perpendicular to it (lateral direction in this study) with a single measurement. The mitigated hardware complexity associated with conventional 3-D ultrasound imaging promises a cheap and small device which will find broad applications, such as detection of metallic markers that are implanted at the site of breast tumours for localisation purposes.

II. Method and Materials

A. Acoustic Signal Received by a Single-Element Transducer

Scattering occurs when the incident wave hits an object smaller than the ultrasound wavelength. Reflections from the scatterer then occur in all directions, giving rise to spherical waves [18] as shown in Fig. 1. For a single-element transducer, the emitted spherical waves from the scatterer is projected onto the transducer aperture, and the received acoustic signal can be approximated by integrating the scattered pressure field over the surface of the transducer, as illustrated in Fig. 2.

The Rayleigh integral has been well established to estimate the radiation pattern of an ultrasound transducer [19], [20]. It

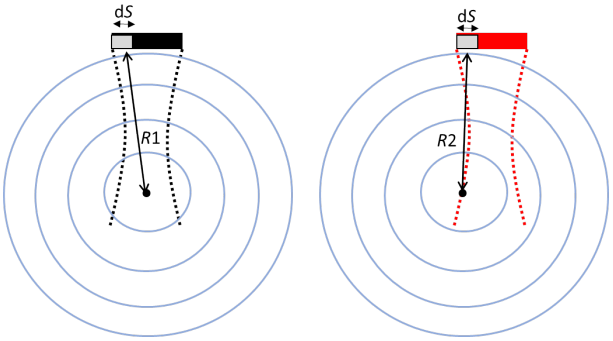

Fig. 2. Schematic illustration of echo reception by a single-element transducer. Depending on the location of the scatterer, the integrated waveform projected onto the receive aperture can be different. The rings indicate the wavefronts.$R1$ and $R2$ are the distances between the scatterer (black point) and the receive sub-aperture $\mathrm{d}S$.

TABLE I
PARAMETERS FOR FIELD II SIMULATIONS

Parameter	Value
Transducer	Single element piston type
Transducer diameter	6 mm
Center frequency	2.4 MHz
Excitation signal	1-cycle sinusoid
Speed of sound	1480 m/s

initially describes the method to obtain the pressure value at a spatial location by summing up the contributions from each radiation sub-aperture when the whole aperture is virtually divided into many tiny elements. Relying on the reciprocity property of wave propagation, the pressure value projected onto the receive aperture, p, is a function of time t, and could be calculated in the time domain by using (1) [20].

$$p(\overrightarrow{r},t) = \rho_0 \int_S \frac{g(\overrightarrow{r}, t-\frac{R}{c})}{2\pi R}\mathrm{d}S, \tag{1}$$

where $\overrightarrow{r}$ indicates the position of the virtual tiny element within the aperture plane, ρ_0 is the density of the medium, g represents the received pressure over the small aperture $\mathrm{d}S$, R indicates the distance between the scatterer and $\mathrm{d}S$, and c is the speed of sound.

We hypothesized that with a single-element transducer, the received pressure field will vary for a scatterer at different lateral positions (Fig. 2).

B. Field II Simulated Pressure Field of a Single-Element Transducer

Field II simulations [21], [22], as given in Fig. 3, are to show the working region for a 2.4 MHz single-element transducer. Table I gives parameters used for the simulations in water. The method does not work in the near field or when the scatterer is located outside the main beam. For example, the beam profile at 10 mm is not suitable for this technique, since there are multiple peaks in the imaging region due to the sidelobes. Beyond 20 mm we can see that sidelobe levels significantly drop. Beyond 30 mm the whole width of the 6-mm transducer (from −3 mm to +3 mm) can be used for this technique.

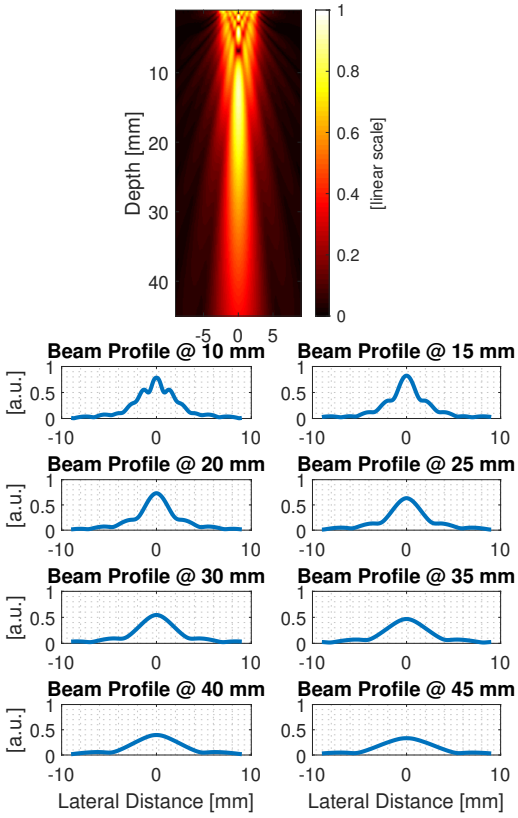

Fig. 3. Field simulations of a single-element transducer with parameters given in Table I.

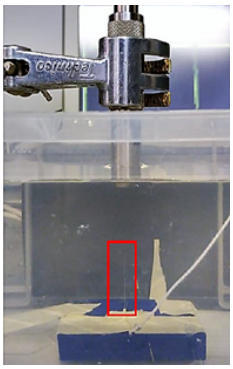

Fig. 4. Experimental setup showing the single-element transducer and the sub-wavelength wire target located at the depth of approximately 40 mm relative to the transducer surface.

C. Experimental Setup

A single-element transducer (Olympus Corporation, USA) with identical parameters as given in Table I was connected to the Ultrasound Array Research Platform (UARP) [23]–

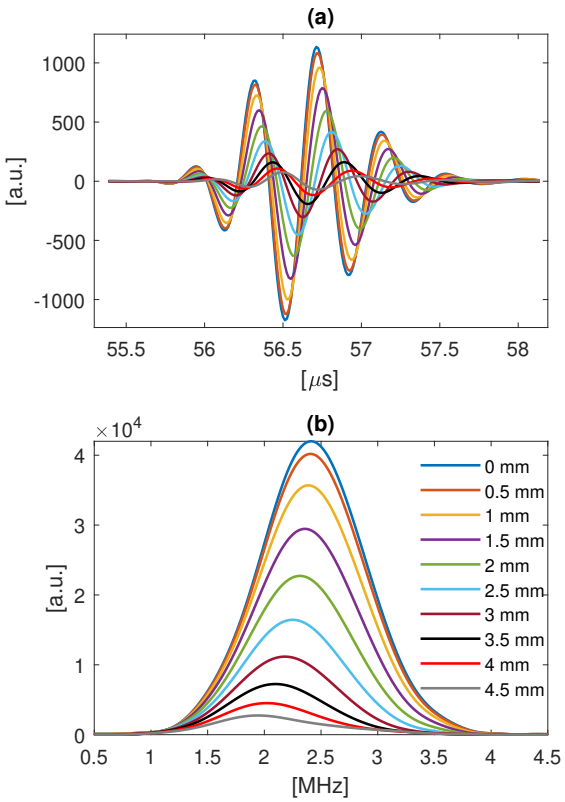

Fig. 5. (a) Reflected echoes from the point scatterer at the depth of 40 mm and varied lateral positions. (b) Corresponding spectra of the acoustic waves shown in (a).

[27] for measurements. A one-cycle sinusoid at 2.4 MHz was generated using a five-level harmonic reduction pulse-width modulation scheme [23], [27] and it was used to excite the transducer with a pulse repetition frequency of 100 Hz. A point scatterer, a 200 μm wire, was placed in front of the transducer in water at a depth of 40 mm as shown in Fig. 4. Measurements were first performed at 40 mm axial distance and 0 mm lateral distance. Later, the transducer was moved by a Zolix stage (Zolix Instruments Co., Ltd., China) in the lateral direction between 0 to 4.5 mm with an incremental size of 0.5 mm, and echoes from the point scatterer were recorded. The nominal minimum distance of movement was 1 μm given by the manufacturer. One hundred pulse-echo measurements were carried out at each location in one procedure, and in total three procedures were performed to verify the repeatability.

D. Experimental Results and Discussion

For measurements at different lateral positions, the peak echo amplitude as shown in Fig. 5 (a) changed according to the beam profile at 40 mm depth shown in Fig. 3, as expected. In addition to the change in peak amplitude, the received echo was filtered by the transducer's spatial response whose characteristic varied with the direction of incidence (a lateral shift). In response to a small change in the lateral position

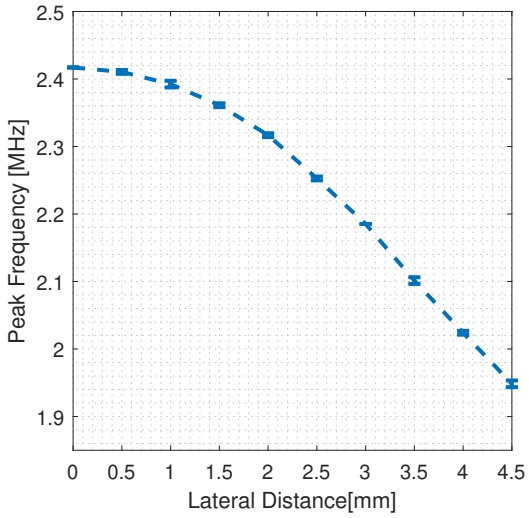

Fig. 6. Repeatability of the measurements shown with the standard deviation error bars plotted at each lateral position. The error bars show the variations between 3 procedures as explained in Section II-C.

(smaller than the wavelength), this spatial filtering effect was significant enough to alter the time domain signal and shift the main peak in the frequency spectrum (Fig. 5). This peak frequency shift can be detected to measure the lateral location of the scatterer (Fig. 6). Besides, the axial location of the scatterer was determined by the time-of-flight measurement. After performing the initial calibration by varying the lateral position of the scatterer, the procedure was repeated for 3 times as mentioned in Section II-C and the repeatability of the method at each lateral position was calculated, as shown in Fig. 6 with the standard deviation error bars.

The results show that multi-dimensional information could be obtained through a single A-mode scan, and in this work, we demonstrated this in 2D (axial dimension and a direction perpendicular to it). The current results could be extended to 3D by breaking the surface symmetry of the sensor through placing a coding mask in front of it, so that the field diversity is introduced and the position of the scatterer can be detected in the third dimension. To unambiguously resolve the signals for each spatial location, robust reconstruction algorithms also need to be further investigated.

III. Conclusion

Efforts are being devoted to the development of cheap and miniature devices for 3-D ultrasound imaging. Differs from the compressed sensing strategy with a mechanically rotating mask placed in front of a single-element transducer, we propose to use the peak frequency shift to localize scatterers in multiple dimensions using the recorded signals with a single-element transducer and single measurement.

IV. Acknowledgement

L. Nie would like to acknowledge support from the U.K. EPSRC under grant EP/P023266/1.

REFERENCES

[1] T. L. Szabo, *Diagnostic Ultrasound Imaging: Inside Out*. Academic Press, 2004.

[2] J. Provost, C. Papadacci, J. E. Arango, M. Imbault, M. Fink, J.-L. Gennisson, M. Tanter, and M. Pernot, "3d ultrafast ultrasound imaging in vivo," *Physics in Medicine & Biology*, vol. 59, no. 19, p. L1, 2014.

[3] J.-l. Gennisson, J. Provost, T. Deffieux, C. Papadacci, M. Imbault, M. Pernot, and M. Tanter, "4-d ultrafast shear-wave imaging," *IEEE Transactions on Ultrasonics, Ferroelectrics, and Frequency Control*, vol. 62, no. 6, pp. 1059–1065, 2015.

[4] M. F. Rasmussen, T. L. Christiansen, E. V. Thomsen, and J. A. Jensen, "3-d imaging using row-column-addressed arrays with integrated apodization-part i: Apodization design and line element beamforming," *IEEE Transactions on Ultrasonics, Ferroelectrics, and Frequency Control*, vol. 62, no. 5, pp. 947–958, 2015.

[5] M. Flesch, M. Pernot, J. Provost, G. Ferin, A. Nguyen-Dinh, M. Tanter, and T. Deffieux, "4d in vivo ultrafast ultrasound imaging using a row-column addressed matrix and coherently-compounded orthogonal plane waves," *Physics in Medicine & Biology*, vol. 62, no. 11, p. 4571, 2017.

[6] A. Austeng and S. Holm, "Sparse 2-d arrays for 3-d phased array imaging-design methods," *IEEE Transactions on Ultrasonics, Ferroelectrics, and Frequency Control*, vol. 49, no. 8, pp. 1073–1086, 2002.

[7] B. Diarra, M. Robini, P. Tortoli, C. Cachard, and H. Liebgott, "Design of optimal 2-d nongrid sparse arrays for medical ultrasound," *IEEE Transactions on Biomedical Engineering*, vol. 60, no. 11, pp. 3093–3102, 2013.

[8] E. Roux, A. Ramalli, P. Tortoli, C. Cachard, M. C. Robini, and H. Liebgott, "2-d ultrasound sparse arrays multidepth radiation optimization using simulated annealing and spiral-array inspired energy functions," *IEEE Transactions on Ultrasonics, Ferroelectrics, and Frequency Control*, vol. 63, no. 12, pp. 2138–2149, 2016.

[9] S. Harput, K. Christensen-Jeffries, A. Ramalli, J. Brown, J. Zhu, G. Zhang, C. H. Leow, M. Toulemonde, E. Boni, P. Tortoli *et al.*, "3-d super-resolution ultrasound imaging with a 2-d sparse array," *IEEE Transactions on Ultrasonics, Ferroelectrics, and Frequency Control*, vol. 67, no. 2, pp. 269–277, 2019.

[10] S. Harnut, K. Christensen-Jeffries, J. Brown, J. Zhu, G. Zhang, C. H. Leow, M. Toulemonde, A. Ramalli, E. Boni, P. Tortoli *et al.*, "3-d super-resolution ultrasound imaging using a 2-d sparse array with high volumetric imaging rate," in *2018 IEEE International Ultrasonics Symposium (IUS)*. IEEE, 2018, pp. 1–9.

[11] G. M. Treece, A. H. Gee, R. W. Prager, C. J. Cash, and L. H. Berman, "High-definition freehand 3-d ultrasound," *Ultrasound in Medicine & Biology*, vol. 29, no. 4, pp. 529–546, 2003.

[12] J. Zhu, E. M. Rowland, S. Harput, K. Riemer, C. H. Leow, B. Clark, K. Cox, A. Lim, K. Christensen-Jeffries, G. Zhang *et al.*, "3d super-resolution us imaging of rabbit lymph node vasculature in vivo by using microbubbles," *Radiology*, vol. 291, no. 3, pp. 642–650, 2019.

[13] C. H. Leow, N. L. Bush, A. Stanziola, M. Braga, A. Shah, J. Hernández-Gil, N. J. Long, E. O. Aboagye, J. C. Bamber, and M.-X. Tang, "3-d microvascular imaging using high frame rate ultrasound and asap without contrast agents: Development and initial in vivo evaluation on nontumor and tumor models," *IEEE Transactions on Ultrasonics, Ferroelectrics, and Frequency Control*, vol. 66, no. 5, pp. 939–948, 2019.

[14] P. Kruizinga, P. van der Meulen, A. Fedjajevs, F. Mastik, G. Springeling, N. de Jong, J. G. Bosch, and G. Leus, "Compressive 3d ultrasound imaging using a single sensor," *Science Advances*, vol. 3, no. 12, p. e1701423, 2017.

[15] P. van der Meulen, P. Kruizinga, J. G. Bosch, and G. Leus, "Coding mask design for single sensor ultrasound imaging," *IEEE Transactions on Computational Imaging*, vol. 6, pp. 358–373, 2019.

[16] J. Janjic, P. Kruizinga, P. Van Der Meulen, G. Springeling, F. Mastik, G. Leus, J. G. Bosch, A. F. van der Steen, and G. van Soest, "Structured ultrasound microscopy," *Applied Physics Letters*, vol. 112, no. 25, p. 251901, 2018.

[17] P. van der Meulen, P. Kruizinga, J. G. Bosch, and G. Leus, "Joint optimization of coding mask and scan positions for compressive single sensor imaging," in *2018 IEEE International Ultrasonics Symposium (IUS)*. IEEE, 2018, pp. 1–4.

[18] P. R. Hoskins, K. Martin, and A. Thrush, *Diagnostic Ultrasound: Physics and Equipment*. CRC Press, 2019.

[19] E. E. Franco, M. A. Andrade, J. C. Adamowski, and F. Buiochi, "Acoustic beam modeling of ultrasonic transducers and arrays using the impulse response and the discrete representation methods," *Journal of the Brazilian Society of Mechanical Sciences and Engineering*, vol. 33, no. 4, pp. 408–416, 2011.

[20] Y. Qian and N. Harrisa, "Direct solution of the rayleigh integral to obtain the radiation pattern of an annular array ultrasonic transducer," *Procedia Engineering*, vol. 47, pp. 861–864, 2012.

[21] J. A. Jensen, "Field: A program for simulating ultrasound systems," in *10TH NORDICBALTIC CONFERENCE ON BIOMEDICAL IMAGING, VOL. 4, SUPPLEMENT 1, PART 1: 351–353*. Citeseer, 1996.

[22] J. A. Jensen and N. B. Svendsen, "Calculation of pressure fields from arbitrarily shaped, apodized, and excited ultrasound transducers," *IEEE Transactions on Ultrasonics, Ferroelectrics, and Frequency Control*, vol. 39, no. 2, pp. 262–267, 1992.

[23] D. Cowell and S. Freear, "Quinary excitation method for pulse compression ultrasound measurements," *Ultrasonics*, vol. 48, no. 2, pp. 98–108, 2008.

[24] P. R. Smith, D. M. Cowell, and S. Freear, "Width-modulated square-wave pulses for ultrasound applications," *IEEE Transactions on Ultrasonics, Ferroelectrics, and Frequency Control*, vol. 60, no. 11, pp. 2244–2256, 2013.

[25] P. R. Smith, D. M. Cowell, B. Raiton, C. V. Ky, and S. Freear, "Ultrasound array transmitter architecture with high timing resolution using embedded phase-locked loops," *IEEE Transactions on Ultrasonics, Ferroelectrics, and Frequency control*, vol. 59, no. 1, pp. 40–49, 2012.

[26] E. Boni, C. Alfred, S. Freear, J. A. Jensen, and P. Tortoli, "Ultrasound open platforms for next-generation imaging technique development," *IEEE Transactions on Ultrasonics, Ferroelectrics, and Frequency Control*, vol. 65, no. 7, pp. 1078–1092, 2018.

[27] D. M. Cowell, P. R. Smith, and S. Freear, "Phase-inversion-based selective harmonic elimination (pi-she) in multi-level switched-mode tone- and frequency-modulated excitation," *IEEE Transactions on Ultrasonics, Ferroelectrics, and Frequency Control*, vol. 60, no. 6, pp. 1084–1097, 2013.